STRUCTURAL AND MORPHOLOGICAL PROPERTIES OF SPUTTERED SILVER OXIDE THIN FILMS: THE EFFECT OF THIN FILM THICKNESS

A. H. HAMMAD[a,b*], M. SH. ABDEL-WAHAB[a], A. ALSHAHRIE[a,c]
[a]*Center of Nanotechnology, King Abdulaziz University, Jeddah, Saudi Arabia*
[b]*Electron Microscope and Thin Films Department, Physics Division, National Research Centre, 33 ElBuhouth St., Dokki, Giza, Egypt.*
[c]*Deptartment of Physics, Faculty of Science, King Abdulaziz University, Jeddah, Saudi Arabia*

Silver oxide thin films were deposited by sputtering the silver metal on glass substrates in flow of O_2/Ar gas. The thin film thickness changed from 54 to 236 nm as the sputtering time changes. Both of the X-ray diffraction and the scanning electron microscopy studies show the dependence of the film structure on the film thickness. Silver oxide exists in different crystalline phases. The lowest as-deposited film thickness has major phase Ag_2O. By increasing the film thickness, Ag_2O_3 phase becomes major phase beside Ag_2O. The annealing films at 250°C shows both of Ag_2O and Ag_2O_3 phases beside Ag metal phase. Furthermore, Ag_2O_3 phase appears as tiny phase at film thickness of 116 and 180 nm. The surface morphology of such films reveals different shapes. Fine crystallites, big particles were observed besides dominating like-sheets through all samples.

(Received September 29, 2016; Accepted November 16, 2016)

Keywords: DC sputtering; silver oxide; XRD; SEM.

1. Introduction

Binary silver oxide [1, 2] can be divided into different compounds such as AgO, Ag_2O, Ag_2O_3, Ag_3O_4 [3], and Ag_4O_3 [4]. Ag_2O_3 can be decomposes into Ag_2O and Oxygen [3]. Ag_3O_4 and Ag_2O_3 were prepared by anodic oxidation of silver salt solutions at lower potentials [3]. Ag_3O_4 is more stable than Ag_2O_3 and filtered as plate like, metallic, or black crystals. It decomposes to AgO at 63 °C [3]. The structural units of Ag_3O_4 is AgO_4 linked together through corners and edges to form 3D network in which oxygen connects three silver ions giving $AgO_{4/3}$ [3].

On the other hand, Ag_4O_3 phase is known as an intermediate phase which can be formed from the electrochemical deposition of AgO [4]. The extended X-ray absorption fine structure spectroscopy (EXAFS) suggested that the formation of Ag_4O_3 phase comes from the electrochemical oxidation of Ag, AgO, or Ag_2O [4].

Otherwise, AgO phase is stable at high oxygen pressure and at low temperature with different crystal structures (cubic, monoclinic, and tetragonal) while Ag_2O has cubic structure [1, 5]. Also, AgO has lower resistance than Ag_2O phase [4]. Wang et al. reported that Ag_2O can be used as a highly efficient photocatalyst to organic contaminants decomposition under visible-light irradiation [5]. So, Ag_2O is photo-decomposes to metallic Ag and O_2 [6]. Furthermore, Ag_2O behave photoconductor with optical band gap of 1.2 eV [7] and 3.32 eV [8] depending on the preparation conditions. However, the reported optical band gap values for the mixture phases (AgO and Ag_2O) are lying in the range from 2.4 to 2.7 eV [9].

Most of the scientific articles are dealt with the preparations of silver oxide thin films by the sputtering or the evaporation silver films followed by an oxidation in a reactive environment [10, 11], i.e. the reactive plasma excited by microwave [12] or by D.C. magnetron sputtering [13].

Farhat and Kandare [14] had prepared AgO thin films by oxidation of Ag in oxygen plasma. They found that the stoichiometric ratio of O/Ag was 1.12. Also, the estimated diffusion coefficient of oxygen in AgO was 5.3×10^{-10} cm^2/day. The activation energy of such films was 0.1

*Corresponding author: ahosny2005@gmail.com

eV. Unfortunately, the AgO films were unstable and decomposed to form Ag_2O after several days. Hence, Mitaray et al. [15], proposed the following reaction to form the stoichiometric Ag_2O: AgO + Ag = Ag_2O.

Pettersson and Snyder [13] investigated the oxidation process of silver thin films prepared by R.F. Sputtering or by thermal evaporation and exposed these films to an oxygen plasma. The refractive index values of such films were found to be greater than 2. The film thickness of the silver oxide is twice of the film thickness of silver. Moreover, they proved that oxide films obtained from sputtering Ag in O_2 have refractive index (2.5) higher than the oxidized of silver films.

Another specific study of polycrystalline sliver oxide (Ag_2O) thin films has been obtained by deposition of silver films by vacuum thermal evaporation and then oxidizing these films in pure oxygen gas [10]. The prepared films were studied by transmission electron microscopy and electron diffraction technique. Fractal and texture structure were observed. The diffraction rings are indexed to Ag_2O phase ({002}, {$1\bar{1}3$}, and {004}) while the texture axis is [110].

The present study is a complementary investigation of silver oxide thin films obtained by DC magnetron sputtering technique at different deposition times in order to know the influence of silver in both of oxygen and argon atmosphere. Extending studies by X-ray diffraction (XRD), and scanning electron microscopy (SEM), were obtained on the as-deposited and the annealed films to provide some important physical parameters and constants such as crystal structure, and morphological surface of the studied films.

2. Experimental details

Silver oxide thin films were deposited on glass substrates using DC magnetron sputtering (DC/RF Magnetron Sputter System, Syskey Technologies- Taiwan). The glass slides were cleaned with acetone and deionized water several times then dried using nitrogen gas before the deposition process. For the deposition studies, High purity (99.999%) target for Ag (3×0.6 inch) metal was used. The plasma was generated inside the sputtering chamber by applying fixed DC power of 100 W for Ag target with fixed oxygen and argon flow rates at 40 and 20 sccm, respectively. The deposition time is varied as 150, 300, 450 to 600 sec. The base pressure in the chamber was adjusted to 1×10^{-6} Torr before introducing Argon gas. The operating pressure of 5×10^{-3} Torr is then maintained with substrate rotation at 15 r/min.

Thin film thicknesses were measured by surface profiler, DektakXT, Bruker, Germany. Table 1 describes the preparation condition of the studied films.

Table 1. Sputtering conditions for deposition of silver oxide thin films.

Sample	Deposition time (s)	Film thickness (nm)	O_2 gas flow rate (sccm)	Ar gas flow rate (sccm)
Ag1	150	54	40	20
Ag2	300	116		
Ag3	450	180		
Ag4	600	236		

X- ray diffraction (type Ultima-IV; Rigaku, Japan) operating at 40 kV and 40 mA with Cuk_α radiation (λ=0.154056 nm), was used to characterize the crystalline phases of the prepared films within 2θ from 20 to 80°.

The morphological microstructure surfaces of the prepared films were investigated by field emission scanning electron microscope (FESEM) (JSM- 7600F; JEOL-Japan). The samples were coated with thin layer of conductive gold before investigation.

3. Results and discussion

3.1 XRD investigation of the as-depositing and annealing sputtered silver oxide films

Fig. 1 shows the XRD spectrum for the as-deposited films at different thicknesses. The observed major phases are cubic Ag_2O and orthorhombic Ag_2O_3. Also, there is a weak peak for all films at about ~ $2\theta = 30.3^{\circ}$ indicating to the AgO monoclinic phase. For silver oxide film at high thickness (236 nm), extra weak peaks at $2\theta = 64.6^{\circ}$ and 77.5° are detected and it represents the cubic sliver metal. Hence, each film thickness shows different planes of AgO, Ag_2O, Ag_2O_3 and Ag. Table 2 represents the collective data of the studied films and their JCPDS numbers.

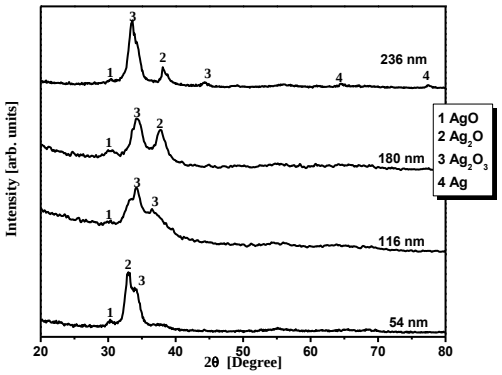

Fig. 1 XRD of the as-deposited silver oxide films under different thicknesses.

Table 2 Crystal structure, crystallite size (D), the strain function (ε), and the dislocation density (δ) of the as-deposited sputtered films

Phase	Ag1	Ag2	Ag3	Ag4	JCPDS number
			Ag_2O_3		
Plane	(040)	(040)	(040)	(311)	
D (nm)	3.38	4.00	4.35	5.59	00-040-0909
ε	0.0086	0.0308	0.0282	0.0225	
δ $(nm)^{-2}$	0.0875	0.0625	0.0528	0.0320	
			Ag_2O		
Plane	(111)	-	(200)	(200)	
D (nm)	10.23	-	5.04	7.93	00-001-1041
ε	0.0106	-	0.0222	0.0140	
δ $(nm)^{-2}$	0.0009	-	0.0393	0.0159	
			AgO		
Plane			(110)		
D (nm)	8.38	5.96	4.06	2.47	00-022-0472
ε	0.0165	0.0232	0.0339	0.0140	
δ $(nm)^{-2}$	0.0142	0.0282	0.0606	0.1640	
			Ag		
Plane	-	-	-	(311)	
D (nm)	-	-	-	17.15	00-001-1164
ε	-	-	-	0.0034	
δ $(nm)^{-2}$	-	-	-	0.0034	

For low films thickness (54 nm), the main major phase is cubic Ag_2O. The peak of Ag_2O has a sharp shoulder at around $2\theta = 34^{\circ}$ and Ag_2O_3 phase can be observed. At 116 nm film thickness, the observed peak is more broadening than at 54 nm. Also, the major phase is Ag_2O_3. By increasing the deposition time / film thickness (450 sec / 180 nm), the film has two major phases Ag_2O_3 and Ag_2O. While at the highest thickness (236 nm), the phase of Ag_2O is sharply

reduced in the intensity value and the major phase is Ag_2O_3. Beside these two phases, new weak peaks at $2\theta = 64.37^{\circ}$ and 77.33° indicating to the presence of Ag metal but with very low ratio.

Scherrer equation is always used to calculate the size of the crystallite (D) and it is depending on both of the full width at half maximum of the diffracted peak (β) in radian unit and the Bragg angle (θ) [16]:

$$D = \frac{0.89\lambda}{\beta\cos\theta} = \frac{0.1371}{\beta\cos\theta} \text{ nm} \quad (1)$$

Also, the strain function (ε), and the dislocation density (δ) [17,18] are calculated for the studied films in order to interpret the silver oxide mechanism or formation as follows:

$$\varepsilon = \frac{\beta\cos\theta}{4} \quad (2)$$

$$\delta = \frac{1}{D^2} \text{ nm}^{-2} \quad (3)$$

The values of the crystallite size, the strain, and the dislocation density are presented in Table 2. The crystallite size of Ag_2O_3 is observed to increase with increasing the film thickness or the deposition time, while the size of the crystallite is decreased as the film thickness or the deposition time increases for the AgO phase. The general trend for Ag_2O phase is the same as the AgO except at the highest thickness (236 nm). Fig. 2 shows the variation of the crystallite size as a function of film thickness for Ag_2O_3 and AgO.

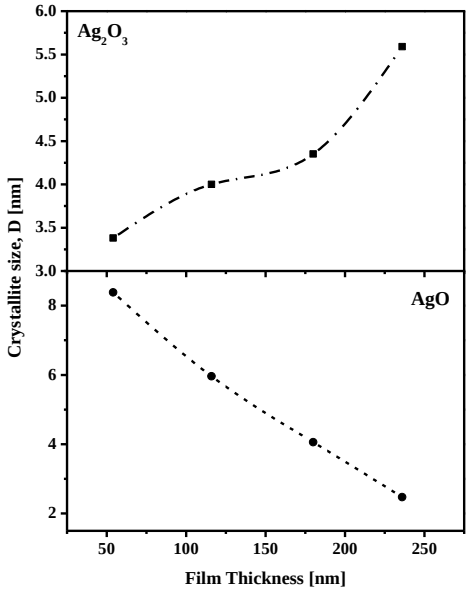

Fig. 2 The dependence of the crystallite size of Ag_2O_3 and AgO on the film thickness.

On the other hand, when the films were annealed at 250 °C for 4 h, the mainly observed phases are Ag_2O and Ag_2O_3 due to their highest peak through the diffraction pattern as shown in Fig. 3. All film samples show sharp and small peaks of Ag metal. Films of thickness 116 and 180 nm have sharp peak of AgO phase at $2\theta \sim 39.5$. The film thickness of 236 nm shows the growth of Ag phase and the phase of AgO disappeared. Table 3 describes the crystal structure, the crystallite size (D), the strain (ε), and the dislocation density (δ) for the annealed films.

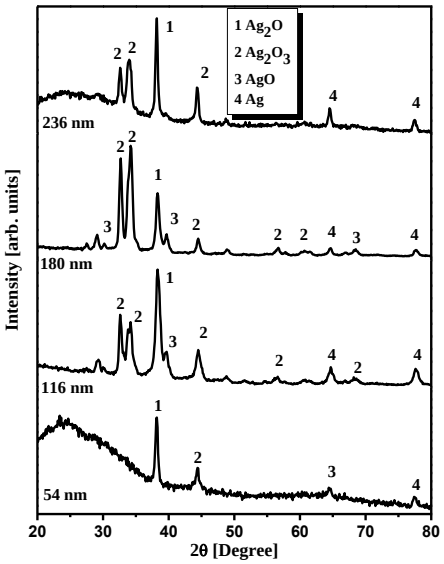

Fig. 3 XRD of the annealing films at 250 °C under different thicknesses.

Table 3 Crystal structure, crystallite size (D), the strain function (ε), and the dislocation density (δ) for the main diffracted peaks of the annealed sputtered films.

Phase	Ag1	Ag2	Ag3	Ag4	JCPDS number
			Ag_2O_3		
Plane			(440)		
D (nm)	17.02	10.57	17.44	21.50	00-040-0909
ε	0.0056	0.0091	0.0055	0.0045	
δ $(nm)^{-2}$	0.0034	0.0089	0.0033	0.0022	
			Ag_2O		
Plane			(200)		
D (nm)	21.06	11.84	15.59	23.27	00-001-1041
ε	0.0053	0.0093	0.0071	0.0048	
δ $(nm)^{-2}$	0.0026	0.0071	0.0041	0.0018	
			AgO		
Plane			$(\bar{2}02)$		
D (nm)	-	10.10	13.11	-	00-022-0472
ε	-	0.0232	0.0082	-	
δ $(nm)^{-2}$	-	0.0282	0.0058	-	
			Ag		
Plane			(311)		
D (nm)	8.65	11.70	15.88	20.2	00-001-1164
ε	0.0067	0.0049	0.0036	0.014	
δ $(nm)^{-2}$	0.0133	0.0073	0.004	0.003	

From the previous results, it can be said that at the specific experimental condition the silver oxide began to deposit as Ag_2O phase. As the result of the presence of atmospheric oxygen, the silver metal target is oxidized giving Ag_2O major phase beside tiny kinks of Ag_2O_3 and AgO. By increasing the sputtering time (film thickness), the crystallites of Ag_2O_3 are grown and increased in their size from 3.38 nm to 5.59 nm. So, the kink of Ag_2O_3 is converted to another mainly phase beside Ag_2O. The nano-AgO crystallites are observed to decrease with increasing the film thickness or the sputtering time as in Fig. 2. Furthermore, the nanocrystallites of Ag_2O are observed to decrease with increasing the film thickness. Hence, it is suggested that at lower film

thickness (≤54 nm), the sputtered silver metal is oxidized to form Ag_2O nanocrystallites. By increasing the sputtering time the Ag_2O is completely converted to Ag_2O_3 at thickness around 116 nm by the following reaction:

$$Ag_2O + O_2 \rightarrow Ag_2O_3$$

This stage is called the intermediate level because the increasing of the sputtering time leads to increase the film thickness and the Ag_2O_3 will be then the main phase beside the Ag_2O phase but in different plane as shown in Table 2. The highest film thickness at about 236 nm shows very weak of Ag metal due to not all silver metal tends to oxidize. So, it is expected that if the sputtering time exceeds 600 sec, Ag metal phase will be grown in expense of Ag_2O and Ag_2O_3 phases.

When the films were annealed at 250 $^{\circ}$C for 4h, the heat treatment of such films is supporting both of Ag_2O and Ag_2O_3 phases. Beside these two phases the silver metal phase is also grown. At the lowest and the highest film thickness (≤116 nm and 236 nm, respectively) the mainly observed phase is Ag_2O beside Ag_2O_3, while at thickness (180 nm) the phases are inverted as happened in the as-deposited films. Moreover, at the film thicknesses 116 and 180 nm, new diffracted peak of AgO phase is detected at $2\theta \sim 39.5^{\circ}$. So, it may come from the reduction of Ag_2O phase due to the effect heat treatment. This assumption is agreed with the decrease of the crystallite size of Ag_2O during these specific two thicknesses as shown in Table 3.

3.2 Thin films morphological investigation

Fig. 4 represents the surface sections of the as-deposited silver oxide thin films. As clearly seen from Fig.4, all samples shows different phases or morphological structures. This result agreed with the XRD study. The lowest film thickness (54 nm) shows fine crystallites titled and aligned in parallel mode. Furthermore, the presence of large sheets and particles are also observed. The tilting of such crystallites, sheets, or particles may be due to specific planes of Ag_2O, Ag_2O_3 and AgO phases. The large sheets have irregular shape for lowest film thickness converted to smooth and regular sheets when the film thickness increases to 116 nm. Also, the fine crystallites number appears more than that observed at lower thickness and randomly distributed through the layers. By increasing the film thickness to 180 nm, the sheets have irregular shapes and aggregates on the surface film. The fine crystallites and the big particles in Ag3 sample are observed to be less than Ag1 sample. The same behavior is also observed for the largest film thickness (236 nm) but with only some few big particles.

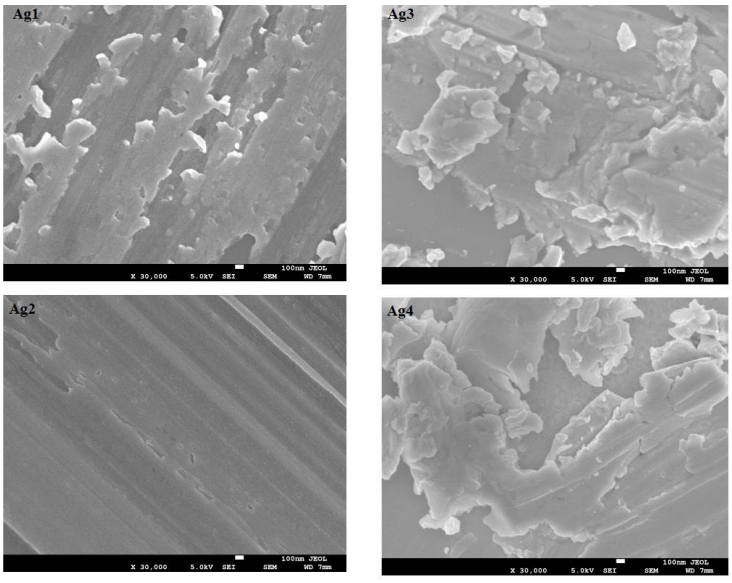

Fig. 4 SEM images of the as-deposited films.

For the annealing films at 450 °C for 4h, the morphological surface is seen to be more clearly and distinguishable as observed in Fig.5. The phase separation phenomenon is also observed through all samples. Hence, different phases are detected in all surface patterns. For the lowest film thickness (54 nm), three types of phases are clearly observed. Fine particles and aggregated small particles are randomly distributed through the surface pattern. Also medium irregular sheets are also presented. These sheets become larger in size for films of thickness (116 nm).

The morphological structure of Ag3 and Ag4 samples is quite different especially the Ag3 sample which has pores. The size of sheets becomes smaller than Ag1 and Ag2 samples. Few fine particles can also be detected. The pores are decreased for films of thickness (236 nm) and the sheets become larger in size.

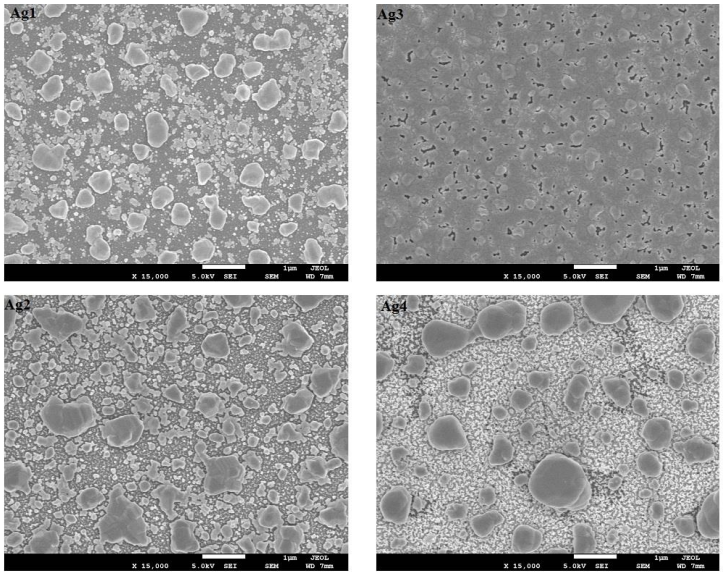

Fig. 5 Morphological surface of the annealing films at 250 °C.

4. Conclusions

Silver metal can be oxidized in O_2/Ar atmospheric flow to form Ag_2O phase at low film thickness or at the beginning of the deposition. Film thickness plays an important role to characterize the silver oxide films. At 116 nm thickness, Ag_2O_3 is the dominating phase although the starting film at 54 nm is Ag_2O. The suggested mechanism is Ag_2O react with O_2 to form Ag_2O_3 phase. At higher film thickness, the observed phases are both of Ag_2O_3 and Ag_2O. The crystallite size of Ag_2O_3 increases as the film thickness increase.

When the films annealed at 250 °C, the silver oxide phases are more distinguished than the as-deposited films. The major phases are also Ag_2O_3 and Ag_2O. The morphological surface for all films shows phase separation on the film surface and sheets shape beside particles and fine crystallites are found. So, under the specific preparation condition, nano-sheets of silver oxide can be formed and the formation Ag_2O_3 may be formed from the oxidation of Ag target.

References

[1] G.A. Kumar, M.V.R. Reddy, K.N. Reddy, Int. Conf. Adv. Nanomater. Emr. Eng. Tech., New Delhi, India, 24th-26th July 2013. pp. 354-356.
[2] L.V. Wüllen, S. Vensky, W. Hoffbauer, M. Jansen, Solid State Sci., **7,** 920 (2005).
[3] B. Standke, M. Jansen, Angew. Chem. Int. Ed. Eng., **25**, 77 (1986).

[4] A.N. Mansour, J. Phys. Chem., **94**, 1006 (1990).
[5] X. Wang, S. Li, H. Yu, J. Yu, S. Liu, Chem. Eur. J., **17**, 7777 (2011).
[6] B. Ohtani, S. W. Zhang, T. Ogita, S. Nishimoto, T. Kagiya, J. Photochem. Photobiol. A, **71**, 195 (1993).
[7] E. Fortiu, F.L. Weichman, Phys. Stat. Sol. B, **5**, 515 (1964).
[8] E. Lund, A. Galeckas, A. Azarov, E.V. Monakhov, B.G. Svensson, Thin Solid Films, **536**, 156 (2013).
[9] H.E. Mehdi, M.R. Hantehzadeh, S. Valedbagi, J. Fusion Energ., **32**, 28 (2013).
[10] S.M. Hou, M. Ouyang, H.F. Chen, W.M. Liu, Z.Q. Xue, Q.D. Wu, H.X. Zhang, H.J. Gao, S.J. Pang, Thin Solid Films, **315**, 322 (1998).
[11] R. Snyders, M. Wautelet, R. Gouttebaron, J.P. Dauchot, M. Hecq, Surf. Coatings Technol., **174-175**, 1282 (2003).
[12] A.I. Boronin, S.V. Koscheev, K.T. Murzakhmetov, V.I. Avdeev, G.M. Zhidomirov, Appl. Surf. Sci., **165**, 9 (2000).
[13] L.A.A. Pettersson, P.G. Snyder, Thin Solid Films, **270**, 69 (1995).
[14] E. Farhat, S.R. Kandare, Thin Solid Films, **23**, 315 (1974).
[15] S. Mitaray, A. Divrechy, A. Donnadieu, Thin Solid Films, **46**, 201 (1977).
[16] G. Gordillo, J.M. Flórez, L.C. Hernández, Sol. Energy Mater. Sol. Cells, **37**, 273 (1995).
[17] A. Sawaby, M.S. Selim, S.Y. Marzouk, M.A. Mostafa, A. Hosny, Physica B, **405**, 3412 (2010).
[18] G.B. Williamson, R.C. Smallman, Philos. Mag., **1**, 34 (1956).